Photodissociation of Isolated Ferric Heme and Heme-His Cations in an Electrostatic Ion Storage Ring

Morten Køcks Lykkegaard, Henning Zettergren, Maj-Britt Suhr Kirketerp, Anneli Ehlerding, Jean Ann Wyer, Umesh Kadhane, and Steen Brøndsted Nielsen*

Department of Physics and Astronomy, University of Aarhus, Ny Munkegade, DK-8000 Aarhus C, Denmark

Received: October 31, 2008; Revised Manuscript Received: December 10, 2008

Photodissociation of isolated Fe(III)-heme$^+$ and Fe(III)-heme$^+$(His) ions in the gas phase has been investigated using an electrostatic storage ring. The experiment provides three pieces of information, namely fragmentation channels, dissociation times, and absorption spectra. After photoexcitation with either 390 or 532 nm light, we find that the fragmentation takes place on a microsecond to millisecond time scale, and the channels are CH_2COOH loss (β-cleavage reaction) and histidine loss from Fe(III)-heme$^+$ and Fe(III)-heme$^+$(His), respectively. These channels were also observed by means of collision-induced dissociation. Significant information on the nonradiative processes that occur after photoexcitation was revealed from the decay spectra. At early times (first two to three milliseconds), the decay of the photoexcited ions is well-described by a statistical model based on an Arrhenius-type expression for the rate constant. The activation energy and preexponential factor are 1.9 ± 0.2 eV and 1×10^{17} to 1×10^{21} s^{-1} for heme$^+$ and 1.4 ± 0.2 eV and 1×10^{16} to 1×10^{19} s^{-1} for heme$^+$(His). Decay on a longer time scale was also observed and is ascribed to the population of lower-lying states with higher spin multiplicity because intersystem crossing back to the electronic ground-state is a bottleneck for the dissociation. The measurements give lifetimes for these lower-lying states of about 10 ms after 390 nm excitation and we estimate the probability of spin flip to be 0.3 and 0.8 for heme$^+$ and heme$^+$(His), respectively.

Introduction

Metalloporphyrins are ubiquitous in nature and are responsible for key biological processes such as photosynthesis, oxygen transport and storage, and sensing.[1−3] They have strong absorption bands in the 380−450 nm (Soret band) and 500−600 nm (Q-band) regions due to $\pi-\pi^*$ transitions in the porphyrin ring. The electronic structure is strongly determined by the presence of a metal and its oxidation and spin state, axial ligands, peripheral substituents, and nearby amino acid residues. One class of metalloporphyrins is heme complexes in which iron is situated in the center of a porphyrin ring. These are found in a number of proteins, the most well-known being myoglobin and hemoglobin.

To elucidate the influence of a protein environment, e.g., nearby amino acid side chains, or water on the photophysics of porphyrins and metalloporphyrins, it is important to study isolated species in the gas phase. In addition, such results are necessary to benchmark excited states calculations, typically carried out on small model systems. Neutrals that are easy to evaporate have been studied extensively by spectroscopic methods[2,4] but there is limited experimental work on ions.[5−7] The latter is somewhat difficult because of a low number of absorbing species and the requirement of special instrumentation.

For gas-phase spectroscopy experiments on ions, we have developed a technique that combines an electrostatic storage ring with an electrospray ion (ESI) source and a tunable pulsed laser system. Daughter ion mass spectroscopy has been made possible by the implementation of pulsed power supplies with microsecond response times for all of the ring elements.[8] The ion current is typically 0.1 pA and with a repetition rate of 10 Hz of the experiment, the number of ions per injection is 1×10^5 when all ions are accumulated in a pretrap. This number is too low to cause a measurable change in the number of photons in the laser pulse, and instead we rely on the detection of ionic fragmentation (i.e., action spectroscopy). The setup allows us to obtain three important pieces of information: ion lifetimes, dissociation channels, and absorption spectra. The advantage of using ESI is that the environment around the chromophore, e.g., heme, can gradually be built up by fine-tuning the source conditions or changing the solution used for electrospraying.

In a recent communication, we reported the absorption spectra of isolated Fe(III)-heme$^+$ and Fe(III)-heme$^+$(His) ions (Figure 1) that provide spectroscopic marker bands in the Soret band region for four-coordinate and five-coordinate heme ions.[9] Here, we follow up on this work but now with emphasis on the dissociation kinetics and fragmentation channels that were only briefly discussed in the previous work. High-energy collision-induced dissociation (CID) experiments were performed at an accelerator mass spectrometer for comparison with the photodissociation mass spectra. Finally, quantum chemical modeling was done to aid in the interpretation of the experimental results.

Experimental Section

CID Experiments. Hemin (Fe(III)-protoporphyrin chloride) was dissolved in CH_2Cl_2/methanol (1:1) to produce heme cations by electrospray ionization.[5] To produce heme$^+$(His) ions, we added histidine to the spray solution. Following ionization, the ions were accelerated to 50 keV kinetic energies, and ions with the m/z of interest were selected by a magnet. After collisions with He, the product ions were measured by an electrostatic analyzer that scanned the kinetic energy of the fragment ions. This resulted in mass-analyzed ion kinetic energy (MIKE)

* Corresponding author. E-mail: sbn@phys.au.dk.

10.1021/jp809626v CCC: $40.75
Published on Web 01/30/2009

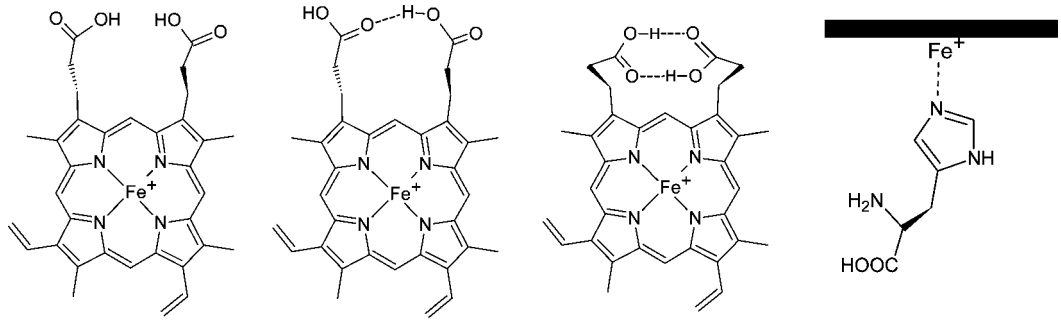

Figure 1. Three structures of Fe(III)-heme$^+$ that differ in the number of hydrogen bonds between the two propionic acid groups (**1**−**3**). The iron atom in Fe(III)-heme$^+$(His) is moved slightly out of the heme plane (black bar) (**4**).

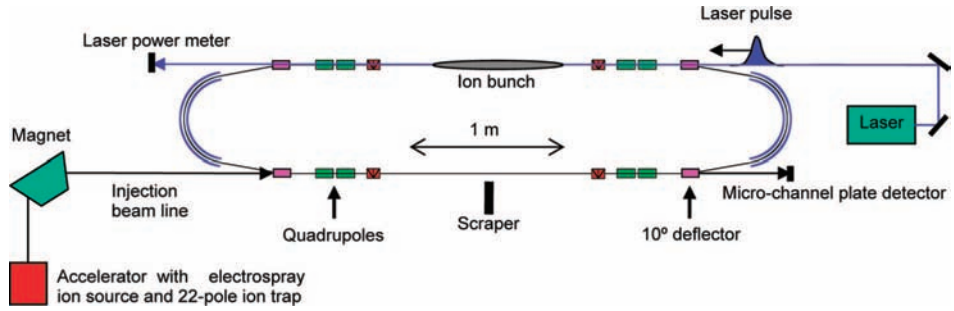

Figure 2. Electrostatic ion storage ring in Aarhus (ELISA) in combination with an ESI source and a laser. The circumference of the ring is 8.3 m. See text for details.

spectra from which the fragment ion masses were identified. More details on the instrumental setup can be found in ref 10.

Storage Ring Experiments. Ions produced by electrospray ionization were accumulated in a 22-pole ion trap in which they were thermally equilibrated with room temperature He gas for 0.1 s. The ion bunch was accelerated to 22 keV, and ions of interest were mass selected before entering ELISA (Figure 2).[8,11] In the ring, the ions have revolution times of ∼100 μs, depending on their mass. After 35 ms of storage time, the bunch was irradiated with light from a pulsed, tunable EKSPLA laser. The laser output is synchronized with the ion trap (10 Hz), and in these experiments we used wavelengths in the 330−532-nm range. Photon absorption led to dissociation into fragment ions and neutral molecules. Neutrals produced on the injection side of the ring were detected with a multichannel plate (MCP) detector. To reach this detector, the ions must survive about half a revolution in the ring (∼50 μs) because ELISA in normal operating mode does not allow fragment ions with lower kinetic energies than that of the parent ion to be stored.

A mass spectrum of the fragment ions was obtained from a quick switch of all ring voltages (within a few microseconds) directly after photoexcitation of the parent ions to store daughter ions with the proper kinetic energy. Daughter ions took about 40 revolutions in the ring before they were dumped on the MCP detector by a fast grounding of the 10° deflector in front of the detector. In other experiments, photoexcited ions were allowed to circulate for ∼100 μs before their fragmentation was monitored. To improve the resolution of the daughter ion mass spectra, a beam scraper on the injection side of the ring was put in to cut off some high energy beam trajectories (see Figure 2).

Computational Details. Calculations were carried out with the GAUSSIAN 03 program package.[12] The geometries of heme$^+$, heme$^+$(His), and smaller fragments were optimized at the B3LYP/6−31G(d) level of theory. Vibrational frequencies were calculated to verify that the stationary points are local minima and not transition states, and frequencies were also used in the calculation of heat capacities for decay modeling. Reaction energies were all corrected for zero-point vibrational energies.

Results and Discussion

First, we consider the results from quantum chemical modeling on heme$^+$ and heme$^+$(His). The electronic ground-state of heme$^+$ was found to be a quartet state in accordance with earlier reports.[13,14] In the case of heme$^+$(His), the quartet electronic state is also lower in energy than doublet and sextet states.

A closer look at the optimized structures reveals that the iron atom in heme$^+$ is located in the plane as opposed to the heme$^+$(His) structure where the iron is displaced a few tenths of an Ångström out of the porphyrin plane to maximize chemical bonding with the histidine. Three different calculated structures of heme$^+$ have been discussed in the literature, and they differ in the number of hydrogen bonds between the two propionic groups, 0, 1, and 2, denoted as structures **1**, **2**, and **3** in Figure 1. We have found that **2** is lower in energy than **1** by 0.3 eV at the B3LYP/6−31G(d) level of theory which is consistent with B3LYP/6−31++G(d,p) calculations by Siu et al.[14] They also found that **3** is lower in energy than **2** by 0.03 eV, but this structure is likely to be entropically disfavored.

The high-energy CID-MIKE spectra of heme$^+$ and heme$^+$(His) after collisions with He are shown in Figure 3. The dominant dissociation channel of heme$^+$ is β-cleavage, which results in loss of one or two CH_2COOH (CMe) groups, each of mass 59. This is in accordance with previous experimental[5,15] and theoretical reports[13] in the literature where β-cleavage is shown to be the lowest energy channel for fragmentation. The other peaks are assigned to loss of one or more side chains of CH_3 (15), $CHCH_2$ (27), COOH (45), CH_2COOH (59) and CH_2CH_2COOH (73) (mass). It is evident from the heme$^+$(His) CID-MIKE spectrum that the dominant dissociation channel is loss of the His ligand of mass 155, which is expected because

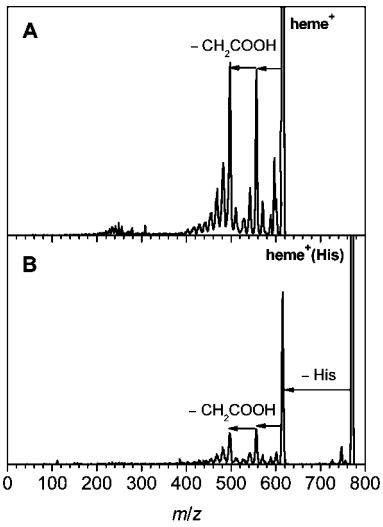

Figure 3. MIKE spectra obtained from collisions between (A) helium and heme$^+$ (*m*/*z* 616) and (B) helium and heme$^+$(His) (*m*/*z* 771).

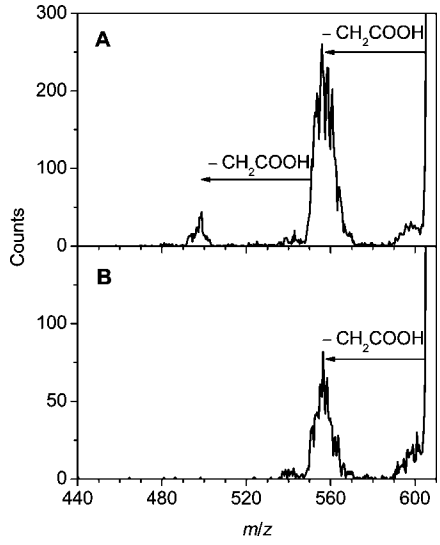

Figure 4. Fragmentation spectra for heme$^+$ acquired (A) at ELISA immediately after photoexcitation with 532 nm light and (B) after storage of the photoexcited ions for one revolution (100 μs).

histidine is bound noncovalently to the iron atom. Earlier multiphoton IR photodissociation experiments on heme$^+$(imidazole) also revealed that imidazole is lost most readily.[7] Significant losses of one or two CMe groups are also seen in the MIKE spectrum. These CID spectra are to be compared with the photodissociation mass spectra taken at ELISA.

Daughter ion mass spectra recorded right after 532-nm photoexcitation of heme$^+$ ions and after a delay of 100 μs are shown in Figure 4. Similar spectra were obtained after 390 nm light absorption (spectra not shown). The resolution is poor ($\Delta m/m \approx 100$) but high enough for identifying the fragment ions from a comparison with the CID spectrum. In the 532 nm spectrum associated with rapid dissociation, 0−20 μs, (cf., Figure 4A), there are two prominent peaks that are due to loss of one or both CMe groups. Two minor peaks are assigned to ions that have lost either H_2O or CH_2CH_2COOH. Delayed dissociation (Figure 4B) also resulted in loss of CMe, H_2O, and CH_2CH_2COOH, whereas a peak due to loss of two CMe groups is absent.

We ascribe the loss of two CMe groups to two-photon absorption because no or few such highly excited ions are

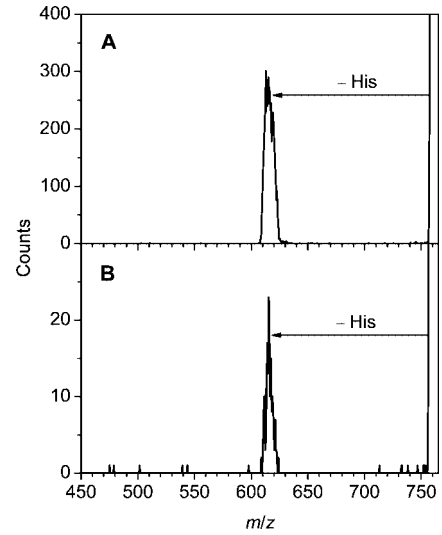

Figure 5. Fragmentation spectra for heme$^+$(His) acquired at ELISA (A) immediately after photoexcitation with 532 nm light and (B) after storage of the photoexcited ions for one revolution (112 μs).

expected to survive the 100 μs delay. This interpretation is in accordance with calculations because one 532 nm photon (2.33 eV) does not possess enough energy to cause two successive β-cleavages. Prior to photon absorption, the ions have an average internal energy of 1.04 eV based on B3LYP/6−31G(d)-calculations of vibrational frequencies and assuming a temperature of 300 K in the ion trap. Hence, after 532 nm photon absorption, the internal energy of the ions is predicted to be 3.37 eV. This is enough for one β-cleavage, calculated to require 2.49 eV (for structure **2**), but not enough for two. Charkin et al.[13] calculated the energies for loss of one and two CMe groups from structure **1** to be 1.80 and 2.41 eV, respectively, and thus the total energy needed to break both bonds must be at least 4.21 eV, which is more than the calculated internal energy of 3.37 eV. At the B3LYP/6−31G(d) level of theory we find the required energy to be 2.20 eV for loss of one CMe from **1**, 0.4 eV more than Charkin et al.

The peak close to the parent ion may be due to either loss of CH_3 or H_2O. However, we calculated that it requires 4.7 eV to lose CH_3, which is in fair agreement with calculations by Charkin et al.,[13b] and therefore this channel is not open upon one-photon absorption. Instead, we find that H_2O loss from propionic acid only requires 1.8 eV, significantly less than the internal energy of 3.37 eV, not considering the barrier to the reaction.

As in the case for heme$^+$, we found similar fragmentation patterns for heme$^+$(His) after both 390 and 532 nm excitation. The only peak observed was due to loss of histidine (Figure 5). We have calculated the dissociation energy for this process to be 1.18 eV. The average energy prior to excitation is 1.36 eV while after 532 nm light absorption, it is 3.69 eV. Dissociation results in ions with too little excess energy to dissociate further on the time scale of the experiment.

Next, we present the results from lifetime experiments in which the yield of neutrals was measured as a function of time after injection of the ions into the ring. Decay spectra are shown for heme$^+$ and heme$^+$(His) in Figure 6. The high yield of neutrals seen immediately after injection is due to metastable ions that were excited during extraction from the ion trap because of collisions with He buffer gas. However, after some milliseconds the decays were dominated by collisions with residual gas in the ring. After 35 ms, the ions were irradiated by 390 nm light, which resulted in an increased yield of neutrals.

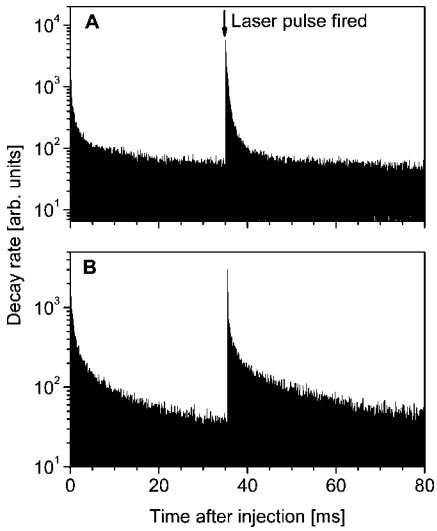

Figure 6. Decay spectra of (A) heme$^+$ and (B) heme$^+$(His). A laser pulse (390 nm photons) was fired after 35 ms.

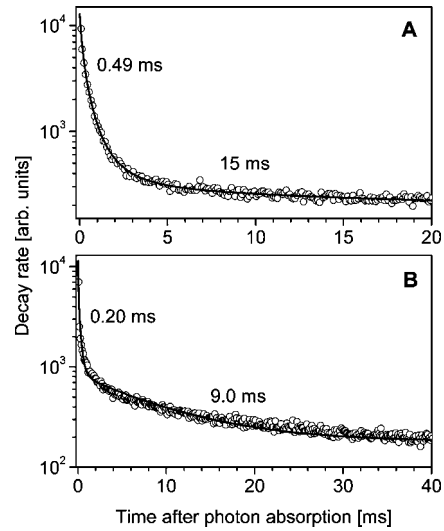

Figure 7. Decay spectra obtained after irradiation of (A) heme$^+$ and (B) heme$^+$(His) with 390 nm light. The spacing of the points is 100 and 112 μs, respectively, which is the revolution time in the ring. The given numbers are the lifetimes.

To describe the observed decays after laser excitation, we use a previously applied model in which the rate constant k is represented by an Arrhenius-like expression[16−18]

$$k(T) = A\exp\left[\frac{-E_a}{k_B(T - E_a/2C)}\right] \quad (1)$$

where T is the microcanonical temperature, C the microcanonical heat capacity, k_B the Boltzmann constant, A the preexponential factor, E_a the activation energy, and $E_a/2C$ is the so-called finite heat-bath correction to the temperature. The average internal energy of the ions before laser excitation was evaluated from an independent harmonic oscillator model with vibrational frequencies obtained from Gaussian calculations. The microcanonical heat capacity C is obtained as the derivative of the microcanonical energy with respect to temperature. The temperature distribution of the ions, $g(T)$, is established in the ion trap and is of the Maxwell−Boltzmann type but is for simplicity approximated by a Gaussian. A final expression for the decay rate of ions in ELISA is then given by

$$I(t) = \int k(T)g(T)\exp[-k(T)t]\,dT \quad (2)$$

The decay of heme$^+$ ions after 390 nm light absorption (Figure 7A) is well-described by eq 2 for the earlier part of the decay, but an additional exponential is required to account for decay at longer times. This analysis gives dissociation lifetimes of 0.49 $\pm$ 0.10 ms and 15 $\pm$ 5 ms. The first time constant is associated with a preexponential factor A of 1×10^{17} to 1×10^{21} s^{-1} and an Arrhenius activation energy E_a of 1.9 $\pm$ 0.2 eV for the β-cleavage reaction. For a simple dissociation reaction, a minimum for the preexponential factor is the transition state constant k_BT/h,[19] where h is Planck's constant. The calculated temperature of heme$^+$ after 390 nm excitation is 648 K and k_BT/h is therefore 1.4×10^{13} s^{-1}. This number is lower than A, which indicates that an increase in entropy is also a driving force for the dissociation reaction.

For heme$^+$(His) (Figure 7B), we have used the same approach and find a preexponential factor of 1×10^{16} to 1×10^{19} s^{-1} and an activation energy of 1.4 $\pm$ 0.2 eV for histidine loss, close to the calculated dissociation energy of 1.2 eV. The fit provides two lifetimes of 0.20 $\pm$ 0.07 ms and 9 $\pm$ 4 ms.

The short lifetime components of sub-milliseconds are the result of internal conversion from the excited state to the electronic ground state with subsequent dissociation of vibrationally excited ions. Here the dissociation itself is the rate-limiting step. The fact that we need an additional exponential with a long lifetime of milliseconds to describe both decays properly is ascribed to a bottleneck for dissociation. Instead of internal conversion directly to the ground state, the ions may undergo intersystem crossing to a lower-lying electronic state with a higher spin. Another spin flip is required to reach the electronic ground state, which is considered to be the rate-limiting step. Thus the ions will eventually relax to the ground-state but with a much smaller rate constant than that for the subsequent dissociation reaction. The second part of the decay is not fully described by an exponential, which is due to the spread in internal energy. It appears here that quite a large fraction of the ions has undergone intersystem crossing, and similar findings were earlier reported for porphyrin ions.[18] We estimate the probability of spin flip after 390 nm excitation from the branching ratio between the two decay channels and found it to be 0.3 $\pm$ 0.1 and 0.8 $\pm$ 0.1 for heme$^+$ and heme$^+$(His), respectively. The difference is likely due to the withdrawal of the iron atom out of the ring by the histidine ligand thereby affecting the electronic structure of the porphyrin ring. We stress that these values are upper limits for the spin flip probabilities because luminescence has been neglected in the analysis.

To fit the experimental data, our initial guesses for the activation energies were the calculated bond energies of 2.49 eV (for structure **2**) and 1.18 eV (structure **4**). These values should in principle give lower limits for the activation energy. However, an acceptable fit to the various heme$^+$ data based on an E_a of 2.49 eV could not be made. A lower value of 1.9 eV was required to account for the tailing at longer times, which suggests that the ions dissociate from structure **1**.

The time scale for histidine deligation is a lower limit when the Fe(III)-heme$^+$ is located in a protein cavity since heat diffusion to the surroundings will occur. The time constant for vibrational cooling is ~4 ps in the case of horse heart cytochrome c as reported by Negrerie et al.[20] on the basis of time-resolved spectroscopy measurements. Indeed, the same authors also report that photodissociation of axial ligands does not occur from ferric heme in this protein in full agreement with the hundred microsecond time scale for dissociation

reported here. The ground-state population was recovered within 20 ps, which was explained by immediate return of photoexcited heme into the hot ground state with subsequent vibrational cooling.[20] In other work, electronic relaxations involving excited states of various origins have been inferred.[21−23] If decay on the millisecond time scale in our experiment is correctly interpreted to be due to trapping in a particular long-lived excited state, it implies that a protein microenvironment provides a doorway to the deexcitation pathway or that it quickly quenches excited states. This issue is to be explored in the future by gradually building the natural heme environment.

Conclusions

In summary, we have used an electrostatic storage ring in combination with a laser to obtain information on the fragmentation channels and dissociation lifetimes of photoexcited Fe(III)-heme$^+$ and Fe(III)-heme$^+$(His) cations. For both ions, dissociation takes place on a microsecond to millisecond time scale, and the main channels are ascribed to loss of CH_2COOH and histidine, respectively. To account for the total decay of ions, both statistical decay and decay delayed by the population of states with different electronic spin has to be included. The time resolution of storage ring experiments is well-suited to disentangling the importance of such competing processes.

Acknowledgment. We thank Prof. Jens Ulrik Andersen for fruitful discussions on the decay modeling. S.B.N. gratefully acknowledges support from the Danish Natural Science Research Council (Grant 272-06-0427), Carlsbergfondet (Grant 2006-01-0229), Villum Kann Rasmussen Fonden, Lundbeckfonden, and Dir. Ib Henriksens Fond.

References and Notes

(1) Berg, J. M.; Tymoczko, J. L.; Stryer L. *Biochemistry*, 6th ed.; W. H. Freeman and Company: New York, 2007.

(2) Makinen, M. W.; Churg, A. K. Structural and Analytical Aspects of the Electronic Spectra of Hemeproteins. In *Iron Porphyrins*; Lever, A. B. P., Gray, H. B., Eds.;; Addison-Wesley: Reading, MA, 1983; Part I.

(3) Kalyanasundaram, K. *Photochemistry of Polypyridine and Porphyrin Complexes*; Academic Press: London, 1997.

(4) Edwards, L.; Dolphin, D. H.; Gouterman, M.; Adler, A. D. *J. Mol. Spectrosc.* **1971**, *38*, 16.

(5) (a) Nonose, S.; Tanaka, H.; Okai, N.; Shibakusa, T.; Fuke, K. *Eur. Phys. J. D* **2002**, *20*, 619. (b) Nonose, S.; Iwaoka, S.; Tanaka, H.; Okai, N.; Shibakusa, T.; Fuke, K. *Eur. Phys. J. D* **2003**, *24*, 335. (c) Nonose, S.; Iwaoka, S.; Mori, K.; Shibata, Y.; Fuke, K. *Eur. Phys. J. D* **2005**, *34*, 315.

(6) (a) Goto, M.; Togawa, M.; Jinno, S.; Takao, T.; Matsumoto, J.; Shiromaru, H.; Achiba, Y.; Tanuma, H.; Azuma, T. *Chem. Phys. Lett.* **2008**, *460*, 46. (b) Goto, M.; Yasuda, Y.; Jinno, S.; Takao, T.; Hanada, K.; Tanuma, H.; Azuma, T.; Sugiura, K.-I.; Shiromaru, H.; Achiba, Y. *Eur. Phys. J. D* **2007**, *43*, 65.

(7) Chiavarino, B.; Crestoni, M. E.; Fornarini, S.; Lanucara, F.; Lemaire, J.; Maître, P.; Scuderi, D. *ChemPhysChem* **2008**, *9*, 826.

(8) Støchkel, K.; Kadhane, U.; Andersen, J. U.; Holm, A. I. S.; Hvelplund, P.; Kirketerp, M.-B. S.; Larsen, M. K.; Lykkegaard, M. K.; Brøndsted Nielsen, S.; Panja, S.; Zettergren, H *Rev. Sci. Instrum.* **2008**, *79*, 023107.

(9) Lykkegaard, M. K.; Ehlerding, A.; Hvelplund, P.; Kadhane, U.; Kirketerp, M.-B. S.; Brøndsted Nielsen, S; Panja, S.; Wyer, J. A.; Zettergren, H *J. Am. Chem. Soc.* **2008**, *130*, 11856.

(10) (a) Larsson, M. O.; Hvelplund, P.; Larsen, M. C.; Shen, H.; Cederquist, H.; Schmidt, H. T *Int. J. Mass Spectrom.* **1998**, *51*, 177. (b) Boltalina, O. V.; Hvelplund, P.; Jørgensen, T. J. D.; Larsen, M. C.; Larsson, M. O.; Sharoitchenko, D. A. *Phys. Rev. A* **2000**, *62*, 023202.

(11) (a) Møller, S. P. *Nucl. Instrum. Methods Phys. Res., Sect. A* **1997**, *394*, 281. (b) Andersen, J. U.; Hvelplund, P.; Brøndsted Nielsen, S.; Tomita, S.; Wahlgreen, H.; Møller, S. P.; Pedersen, U. V.; Forster, J. S.; Jørgensen, T. J. D *Rev. Sci. Instrum.* **2002**, *73*, 1284.

(12) Frisch, M. J.; Trucks, G. W.; Schlegel, H. B.; Scuseria, G. E.; Robb, M. A.; Cheeseman, J. R.; Montgomery, J. A.; Vreven, T.; Kudin, K. N.; Burant, J. C.; Millam, J. M.; Iyengar, J.; Tomasi, J.; Barone, V.; Mennucci, B.; Cossi, M.; Scalmani, G.; Rega, N.; Petersson, G. A.; Nakatsuji, H.; Hada, M.; Ehara, M.; Toyota, K.; Fukuda, R.; Hasegawa, J.; Ishida, M.; Nakajima, T.; Honda, Y.; Kitao, O.; Nakai, H.; Klene, M.; Li, X.; Knox, J. E.; Hratchian, H. P.; Cross, J. B.; Adamo, C.; Jaramillo, J.; Gomperts, R.; Strattman, R. E.; Yazyev, O.; Austin, A. J.; Cammi, R.; Pomelli, C.; Ochterski, J. W.; Ayala, P. Y.; Morokuma, K.; Voth, G. A.; Salvador, P.; Dannenberg, J. J.; Zakrzewski, V. G.; Apprich, S.; Daniels, A. D.; Strain, M. C.; Farkas, O.; Malick, D. K.; Rabuck, A. D.; Raghavachari, K.; Foresman, J. B.; Ortiz, J. V.; Cui, Q.; Baboul, A. G.; Clifford, S.; Cioslowski, J.; Stefanov, B. B.; Liu, G.; Liashenko, A.; Piskorz, P.; Komaromi, I.; Martin, R. L.; Fox, D. J.; Keith, T.; Al-Laham, M. A.; Peng, C. Y.; Nanayakkara, A.; Challacombe, M.; Gill, P. M. W.; Johnson, B.; Chen, W.; Wong, M. W.; Gonzalez, C.; Pople, J. A. *Gaussian 03, Revision B.05*; Gaussian, Inc.: Pittsburgh, PA, 2003.

(13) (a) Charkin, O. P.; Klimenko, N. M.; Nguyen, P. T.; Charkin, D. O.; Mebel, A. M.; Lin, S. H.; Wang, Y.-S.; Wei, S.-C.; Chang, H.-C. *Chem. Phys. Lett.* **2005**, *415*, 362. (b) Charkin, O. P.; Klimenko, N. M.; Charkin, D. O.; Chang, H.-C.; Lin, S.-H. *J. Phys. Chem. A* **2007**, *111*, 9207.

(14) Siu, C.-K.; Guo, Y.; Hopkinson, A. C.; Siu, K. W. M. *J. Phys. Chem. B* **2006**, *110*, 24207.

(15) Van Berkel, G. J.; McLuckey, S. A.; Glish, G. L. *Anal. Chem.* **1991**, *63*, 1098.

(16) Andersen, J. U.; Bonderup, E.; Hansen, K. *J. Chem. Phys.* **2001**, *114*, 6518.

(17) (a) Andersen, J. U.; Cederquist, H.; Forster, J. S.; Huber, B. A.; Hvelplund, P.; Jensen, J.; Liu, B.; Manil, B.; Maunoury, L.; Brøndsted Nielsen, S.; Pedersen, U. V.; Schmidt, H. T.; Tomita, S.; Zettergren, H *Eur. Phys. J. D* **2003**, *25*, 139. (b) Andersen, J. U.; Cederquist, H.; Forster, J. S.; Huber, B. A.; Hvelplund, P.; Jensen, J.; Liu, B.; Manil, B.; Maunoury, L.; Brøndsted Nielsen, S.; Pedersen, U. V.; Rangama, J.; Schmidt, H. T.; Tomita, S.; Zettergren, H *Phys. Chem. Chem. Phys.* **2004**, *6*, 2676. (c) Andersen, L. H.; Bluhme, H.; Boyé, S.; Jørgensen, T. J. D.; Krogh, H.; Nielsen, I. B.; Brøndsted Nielsen, S.; Pedersen, U. V.; Svendsen, A *Phys. Chem. Chem. Phys.* **2004**, *6*, 2617.

(18) (a) Calvo, M. R.; Andersen, J. U.; Hvelplund, P.; Brøndsted Nielsen, S.; Pedersen, U. V.; Rangama, J.; Tomita, S.; Forster, J. S *J. Chem. Phys.* **2004**, *120*, 5067. (b) Nielsen, C. B.; Forster, J. S.; Ogilby, P. R.; Brøndsted Nielsen, S. *J. Phys. Chem. A* **2005**, *109*, 3875.

(19) Laskin, J.; Futrell, J. H. *J. Phys. Chem. A* **2003**, *107*, 5836.

(20) Negrerie, M.; Cianetti, S.; Vos, M. H.; Martin, J.-L.; Kruglik, S. G. *J. Phys. Chem. B* **2006**, *110*, 12766.

(21) Petrich, J.; Poyart, C.; Martin, J. L. *Biochemistry* **1988**, *27*, 4049.

(22) Petrich, J. W.; Martin, J. L.; Houde, D.; Poyart, C.; Orszag, A. *Biochemistry* **1987**, *26*, 7914.

(23) Franzen, S.; Kiger, L.; Poyart, C.; Martin, J. L. *Biophys. J.* **2001**, *80*, 2372.

JP809626V